

# A Study of Van Allen Belt Signatures of Nuclear Weapon Tests for Future CTBT Technologies

F. M. Wach and J. Velthuis

H.H. Wills Physics Laboratory, Tyndall Avenue, Bristol BS8 1TL.

C. A. Steer

Applied Physics, School of Health and Applied Sciences,  
St Mary's University, Waldegrave Rd, Twickenham TW1 4SX.

(Dated: October 18, 2017)

There are a number of measurement techniques employed to enforce the Comprehensive Test Ban Treaty (CTBT), with complementary measurements of seismic and atmospheric radionuclide data being foremost. The potential for decoupling and trapping of radionuclide gases in underground nuclear tests places importance on the identification and characterization of new techniques. Earlier studies of charged particle data in low Earth orbit satellites have shown that seismic events can result in particle bursts, that can be detected. There is strong evidence for the precipitation of charged particles in the van Allen belts caused by seismic events. Particle bursts, that are coincident in time and expected location, in satellite-borne detectors have been observed with a  $>5$ -sigma significance with earthquake activity at the corresponding location in SAMPEX/PET, MARIA/SALYUT-7, GAMMA-1 [1], and DEMETER [2].

In this study, we first identified seismic signals in the data and then electron energy correlations around the times of Democratic People's Republic of Korea (DPRK) nuclear tests. Given the low numbers of DPRK nuclear tests, we first analyzed the data to examine temporal correlations with seismic activity. We observe temporally- and spatially-correlated particle bursts starting just before seismic events and continuing throughout the period of activity. The correlations have a periodic character due to the eccentric GPS satellite orbit, where it dips into and out of the Van Allen belt during the seismic activity. Then we analyzed the times around the DPRK nuclear tests. For a very simple detection method, we find that we are unable to explain the cross-correlations in electron energy channels as being due to natural variability for four out of five DPRK tests. This suggests that the energy band cross-correlations, around the time of DPRK tests, appear to have a distinct character than from all other natural periods (of, say, even seismic activity).

## INTRODUCTION

Many studies have indicated the temporal and spatial correlation of Van Allen particle bursts and seismic activity [1–3]. The mechanism leading to seismically-correlated particle bursts (PBs) is believed to be caused by ultra and extra low frequency (ULF and ELF) wave emissions. The lower atmosphere is transparent at ULF/ELF frequencies so that any generated will propagate to the ionosphere, which is opaque. At the ionosphere, the wave causes oscillations of ionospheric charge. *Sivadas* [3] and *Aleksandrin* [1] discuss the PB origin, and propose that low frequency waves become trapped in a geomagnetic field tube, which are specified by the L-shell number corresponding to the earthquake. Data analysis on the seismic correlations has confirmed that altitudes between 300 and 500 km, within the ionosphere, maximize the correlation significance. The oscillation of the ionospheric charge initiates a magnetohydrodynamic Alfvén wave that travels along the given L-shell interacting resonantly with particles trapped in the Earth's magnetic field. This results in particles precipitating and circulating within their given L-shell for up to 12 hours and an increase in particle flux around the time of seismic activity.

There are many observations supporting the proposed mechanism and its application to Weapons test detection: ULF and ELF waves have been observed near earthquakes [11] and nuclear weapons tests [12]. Separately, ionospheric electron charge fluctuations have been also observed

in coincidence with both seismic activity (see Ref. [9], for example) and early DPRK nuclear device tests [10]. Given these ionospheric fluctuations, and the evidence Van Allen belt particle precipitation occurs near times of seismic activity, we aimed to examine an recently released dataset for Van Allen belt signatures of nuclear weapons tests.

The data for this study was published by the Los Alamos National Laboratory team and comprises the electron and proton rates from 23 GPS satellites between 1<sup>st</sup> January 2001 and 1<sup>st</sup> January 2017. The satellites were equipped with Burst Detector Dosimeters IIR (BDD-IIR) [4] and Combined X-Ray sensor and Dosimeters (CXD) [5] and travelled along a path with a period of approximately 12 hours, taking measurements every 240s. Figure 1 illustrates the trajectories of some of the GPS satellites.

The on-board particle detectors took measurements of rates and fluxes for both electrons and protons as well as recorded geographic locations, magnetic fields and L-shell values. In this analysis we focus mainly on electron rates and their variation in time and within L-shells.

## METHOD

### Correlated particle bursts and surrogate seismic events

In the first seismic part of the project we investigated whether the observations made by low-Earth-orbit satellites

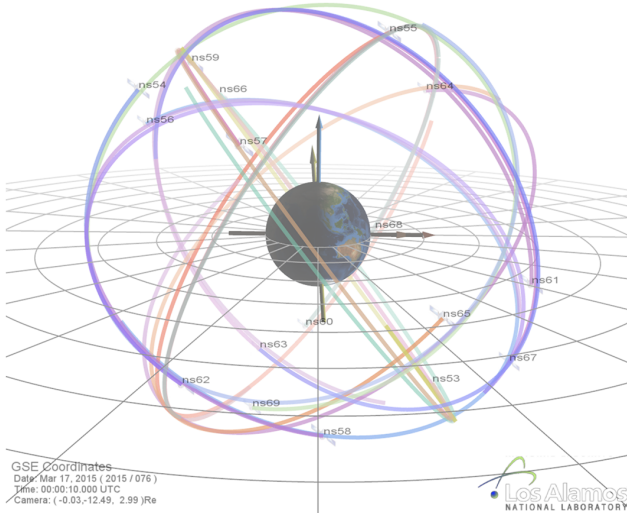


FIG. 1. Trajectories of satellites equipped with CXD instruments (figure reproduced from Ref. [6]).

can also be found in our data. In our analysis we attempted to reproduce the results presented by Aleksandrin *et al.* by improving his analysis method [1].

The data was analysed in two-year chunks and PBs were defined as readings exceeding the average by at least four  $\sigma$  (following the analysis process described in Ref. [1]). Subsequently, PBs were matched to earthquakes (obtained from U.S. Geological Survey) based on the following conditions: the PB occurs within 12 hours before or after the earthquake and that the earthquake L-Shell ( $L_{EQ}$ ) should close to the PB L-shell ( $L_{PB}$ ). The L-shell data cut used here was described by

$$\Delta L = L_{EQ} - L_{PB} < 0.07 \quad (1)$$

Since precipitated particles remain trapped within a given L-Shell for up to 12 hours, we assume that detection of PB depends only on the L-Shells the satellite is traversing regardless of its geographic location.

An important test of the confidence of the correlations was to also study temporal correlations for much larger  $\Delta L$ , which corresponded to looking at regions of the Earth that are seismically inactive. If the PB and earthquake correlations were present only for small  $\Delta L$  then it provides further evidence for the phenomenon.

#### Energy spectrum cross-correlation analysis

In the second part of this work the cross-correlations between detector energy channels was examined. Our method involved investigating normalised cross-correlation coefficients (NCC) and the NCC between energy channels  $E_a$  and

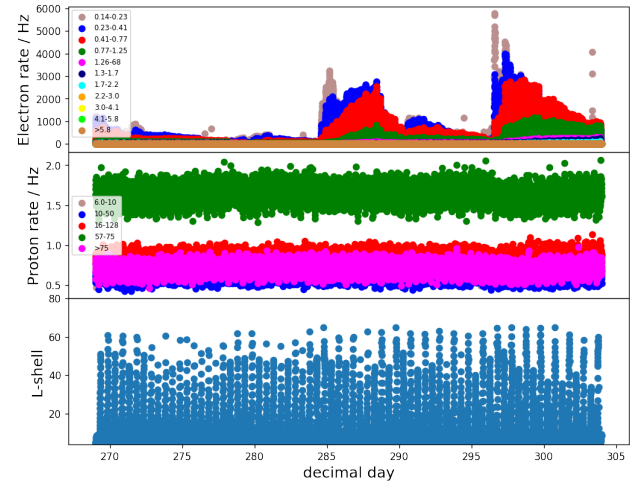


FIG. 2. Figure to show L-Shell, proton and electron rate readings between 24<sup>th</sup> Sept and 31<sup>st</sup> Sept 2010. The legend indicates the energy channel with energy in MeV.

$E_b$  is given by

$$NCC = \frac{\sum_{n=0}^N E_a(n) \sum_{n=0}^N E_b(n)}{\sqrt{\sum_{n=0}^N E_a^2(n) \sum_{n=0}^N E_b^2(n)}}, \quad (2)$$

where  $n$  denotes the index of the data point. The NCCs for fortnightly periods over 16 years of data were obtained. This distribution of NCCs contained the variation of the NCCs for naturally-occurring events, excluding the dates of the DPRK tests. This population of NCCs for naturally-occurring events was used as the baseline for comparison with periods of nuclear testing.

## RESULTS

### Example Data

An example summary plot of the dataset for a week in September, 2010, is shown in Figure 2. The electron rate can be seen to strongly vary in periods of space weather storms, whereas the proton rates in different energy channels can be seen to be quite constant over the time period. In contrast to earlier satellite studies, GPS satellites' trajectories have wide excursions in L-shell, which is related to the magnetic latitude  $\lambda$  and altitude  $r$  by  $L = r \cos^2 \lambda$ , as indicated by the lowest panel of Figure 2.

Figure 3 shows the same data summary collected around the time of one of the DPRK nuclear tests. For this example, and at this particular time, the satellite found itself at a lower L-shell and it can be seen that the test also occurred around the time of a very low energy burst of electrons. The potential for coincidentally finding a burst at the same time as a DPRK nuclear test motivated the use of the NCC method described above, where natural variability in electron energy

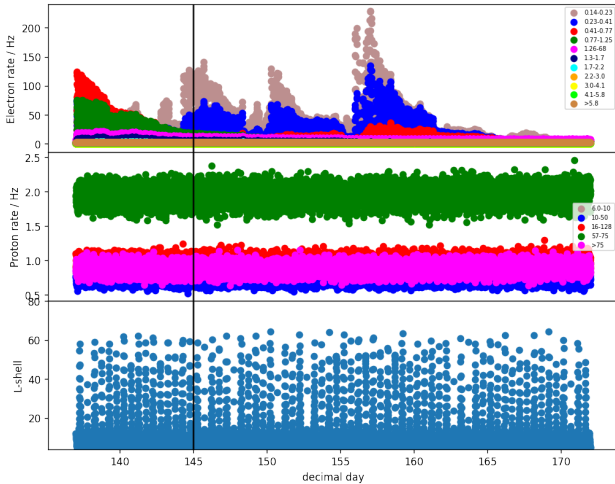


FIG. 3. Electron and proton rates for the test on 25<sup>th</sup> May 2006 (marked by black vertical line).

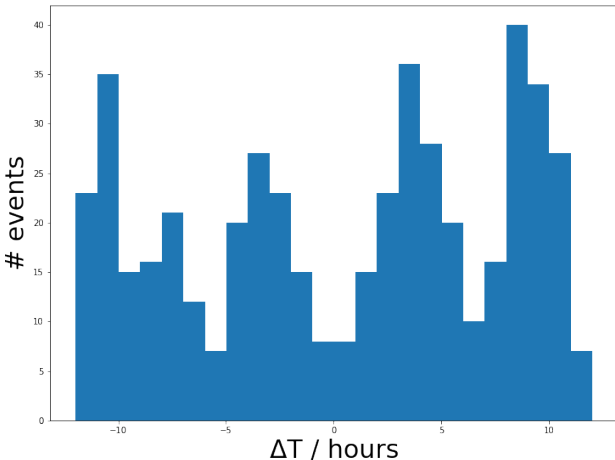


FIG. 4. Temporal correlation histogram for satellite ns56 under the condition  $\Delta L < 0.07$ .

cross-correlation was found before comparing it to periods of nuclear testing.

### Seismic Activity Analysis

An example of a temporal correlation histogram, which measures the time difference between PB and earthquake (that satisfy the L-shell data cuts), is shown in Figure 4 for satellite ns56. The peaks represent particle bursts detected by the satellite that are coincident in time and position (or L-shell) with an earthquake. The peaks appear to be more significant for small  $\Delta L$  than for larger  $\Delta L$  cuts , show in Figure 5. The period of the peaks corresponds to the satellite orbital period, cutting the L-shell twice for every orbit. Also the coupling between the earthquake and PB was typically observed around  $4 < L\text{-shell} < 5$ .

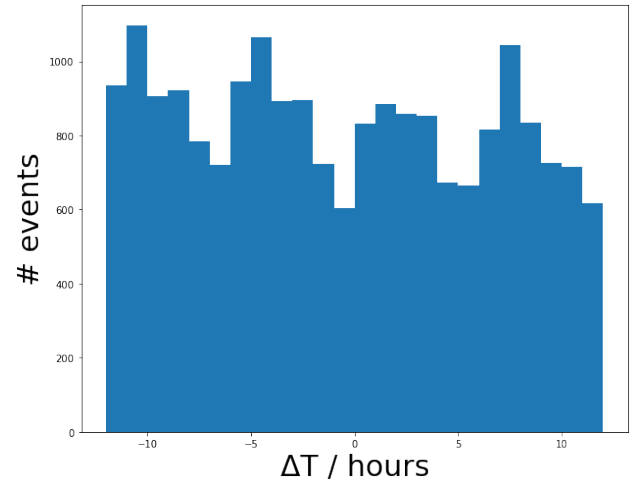


FIG. 5. Temporal correlation histogram for satellite ns56 under the condition  $\Delta L < 1$  .

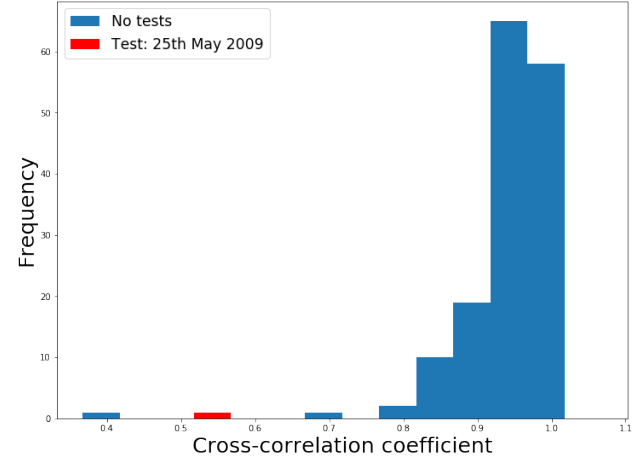


FIG. 6. NCC between channels 2 and 4 for a test performed on 25<sup>th</sup> May 2006 as compared to the values calculated for 16 years of data.

### Energy Cross-Correlation Analysis

The method of energy spectrum cross-correlation analysis appeared to be successful in discerning between nuclear tests from 2006, 2009 and 2013 and naturally occurring phenomena. Figure 6 shows a histogram of how a set of NCCs for a particular test from 25<sup>th</sup> May 2006 compare to the overall population and Table I gives the set of p-values for all the channels for this test as an indicative analysis example.

This method was applied to data collected by five different

Channel	0	1	2	3	4	5	6	7	8	9	10
P-values	0.49	0.72	1.00	0.01	0.01	0.04	0.04	0.07	0.05	0.03	0.03

TABLE I. Table of P-values for NCCs from the test performed on 25<sup>th</sup> May 2006.

	ns54	ns56	ns59	ns60	ns61
Oct 2006	1	0	0	1	1
May 2009	6	2	1	2	2
Feb 2013	3	4	4	2	3
Jan 2016	0	1	0	0	0
Sep 2016	0	0	0	0	0

TABLE II. The number of observed NCC outliers, which have a p-value less than 0.05, for the DPRK tests indicated.

satellites over the full dataset.

Much work needs to be done to develop detection methods, which were broadly out of scope for this study; here we are summarize the analysis so far to indicate whether the technique holds promise. In order to illustrate the technique's potential, we do, however, consider a simplistic method. We use a p-value less than 0.05 to reject the hypothesis that the NCC behaviour could be explained naturally. Table II show the number of outliers for each nuclear test by the satellites. Using this simple method, it can be seen that the first four DPRK tests could not be explained as being due to natural variability in the dataset.

## DISCUSSION

Temporal correlation method appears to produce results confirming previous observations from a low-Earth-orbit satellites mentioned earlier. To be the best of our knowledge it is the first time these effects have been seen in higher-altitude satellite orbits.

The energy spectrum cross-correlation analysis requires more time and focus to either confirm or refute its usefulness. Although promising, and if correct, it could be a very useful tool in detecting nuclear test signatures as various background effects (mainly of the seismic and cosmic orginigs) are already taken into account. The alternative approach to the problem would involve gaining a better understanding of the signal in terms of background and effects of seismic activity on electron and proton rates.

The method of cross-correlations appears promising, showing correlations and patterns that require more attention than is possible in a 3 month study. It is also appears very feasible to extract the nuclear test signatures with a further focus on data analyses and detection algorithms in the future.

## CONCLUSIONS

This analysis has provided very encouraging initial results, that would greatly benefit from further study. Firstly, the analysis presented suggested that it could be used for seismic pre-cursor event analysis as we observed temporally- and spatially-correlated particle bursts and earthquakes. Secondly, the character of energy correlations within particle bursts as-

sociated with nuclear tests appear to be exceptional when compared to natural causes of electron rate variability. Using a very simple detection method, it can be seen that the first four DPRK tests could not be explained as being due to natural variability in the dataset.

- 
- [1] *High-energy charged particle bursts in the near-Earth space as earthquake precursors.* Aleksandrin, et.al., Annales Geophysicae **21**, p. 597–602, (2003).
  - [2] *Burst increases of precipitating electrons recorded by the DEMETER satellite before strong earthquakes.* Zhang., et al., Natural Hazards and Earth System Sciences **13**, 197, (2013).
  - [3] *High Energy Particle Bursts as Seismic Precursors.* N. Sivadas (2010).
  - [4] *A new numerical technique to design satellite energetic electron detectors.* Tuszewski, et al., Nuclear Instruments and Methods in Physics Research Section A: Accelerators, Spectrometers, Detectors and Associated Equipment, p. 653–666, (2002).
  - [5] *Bremsstrahlung effects in energetic particle detectors.* Tuszewski, et al., Space Weather **2.10** (2004).
  - [6] *The Global Positioning System constellation as a space weather monitor: Comparison of electron measurements with Van Allen Probes data.* Morley, et al., Space Weather **14.2**, p. 76–92 (2016).
  - [7] *Description of the BDD-IIR: electron and proton sensors on the GPS Cayton, et al., No. LA-UR-98-1162.* Los Alamos National Lab., NM (United States), 1998.
  - [8] *Monte Carlo Simulation of the Particle Channels of the Combined X-Ray sensor and Dosimeter (CXD) for GPS Block IIR and Block IIF* Cayton, T. , 2004.
  - [9] *Global Positioning System detection and energy estimation of the ionospheric wave caused by the 13 July 2003 explosion of the Soufrière Hills Volcano, Montserrat* Dautermann, et al, Journal of Geophysical Research: Solid Earth, **114**, 2156, (2009).
  - [10] *Global Positioning System detection and energy estimation of the ionospheric wave caused by the 13 July 2003 explosion of the Soufrière Hills Volcano, Montserrat Park*, et al, Journal of Geophysical Research: Solid Earth, **38**, 1944, (2011).
  - [11] *On precursory ULF/ELF electromagnetic signatures for the Kobe earthquake on April 12, 2013* Schekotov, et al, Journal of Asian Earth Sciences, **114**, 305, (2015).
  - [12] *ELF and VLF radio waves*, Barr, et al, Journal of Atmospheric and Solar-Terrestrial Physics, **62**, 1689, (2000).

## APPENDIX

Here we show a full set of histograms showing NCC values for all the energy channels as observed by different satellites for nuclear tests between 2006 and 2016.

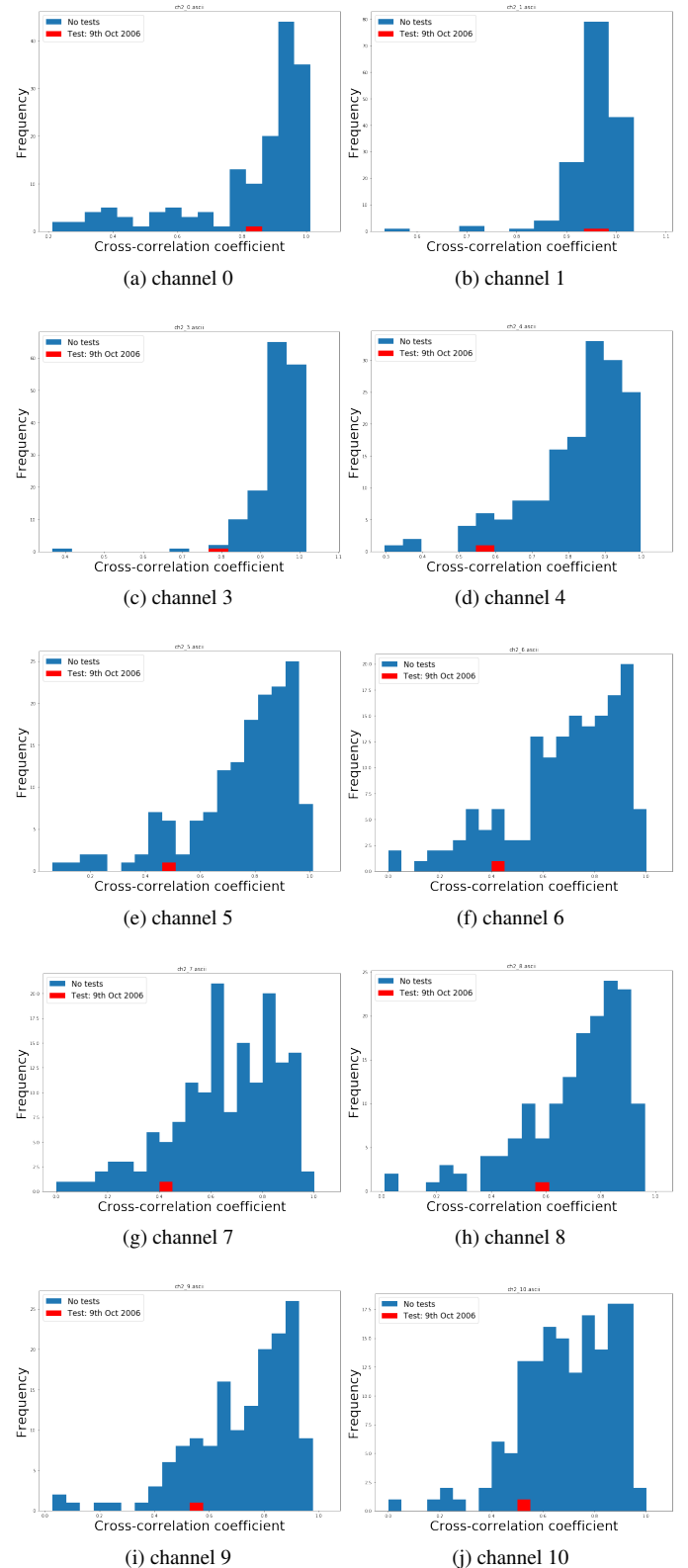


FIG. 7. Normalised cross–correlation coefficients of channel 2 for October 2006 test – satellite ns54.

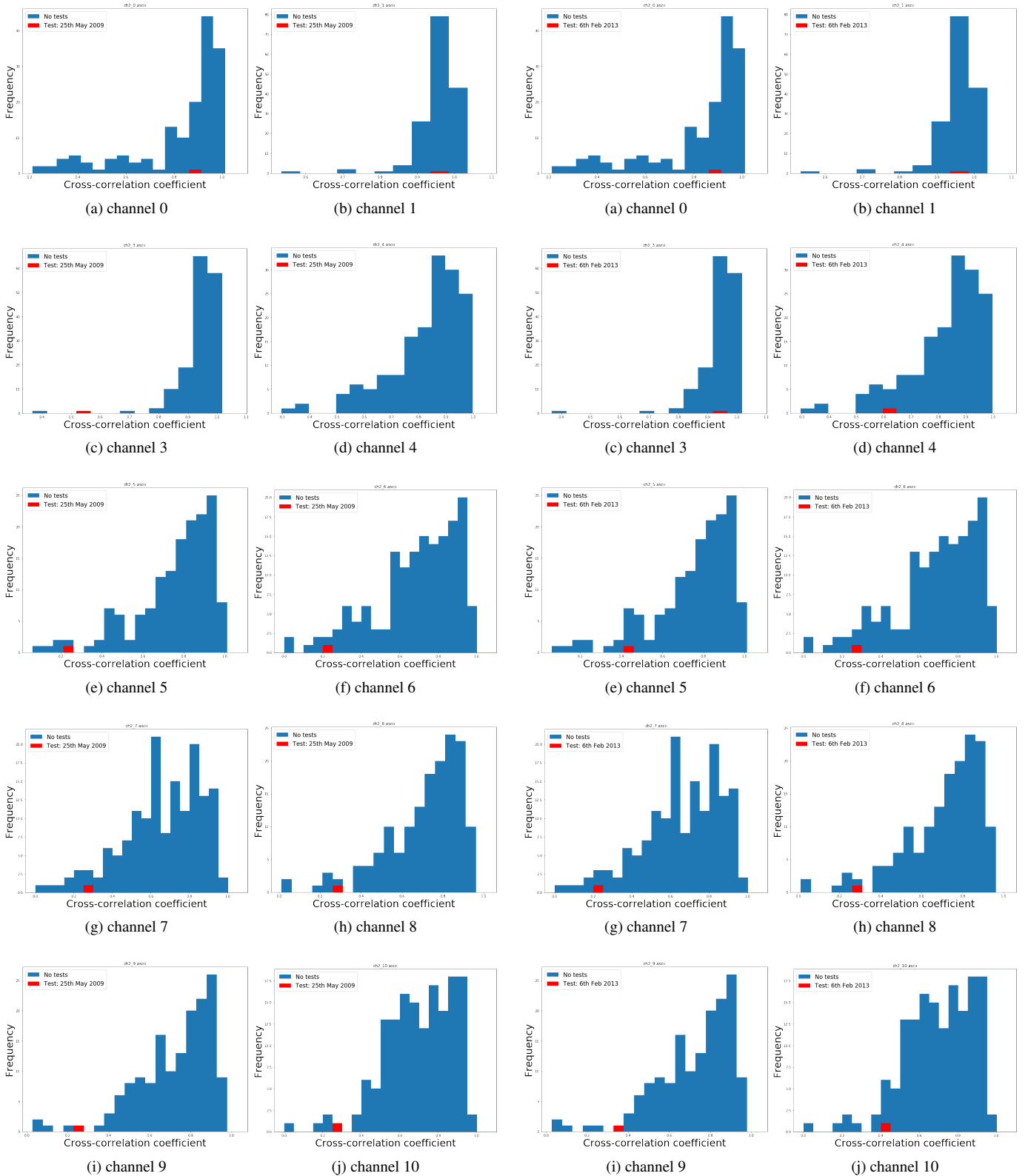


FIG. 8. Normalised cross-correlation coefficients of channel 2 for May 2009 test – satellite ns54.

FIG. 9. Normalised cross-correlation coefficients of channel 2 for February 2013 test – satellite ns54.

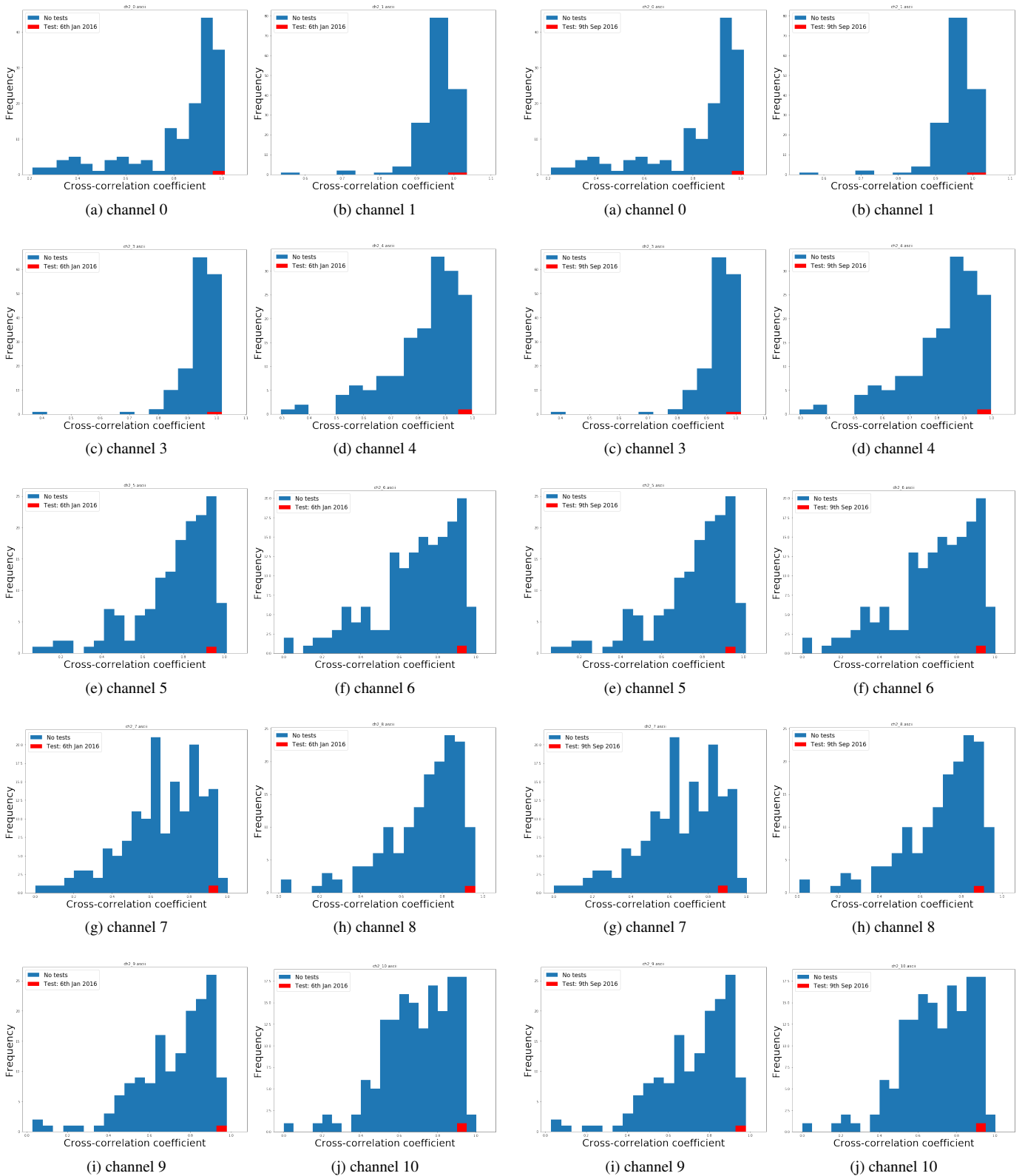


FIG. 10. Normalised cross–correlation coefficients of channel 2 for January 2016 test – satellite ns54.

FIG. 11. Normalised cross–correlation coefficients of channel 2 for September 2016 test – satellite ns54.

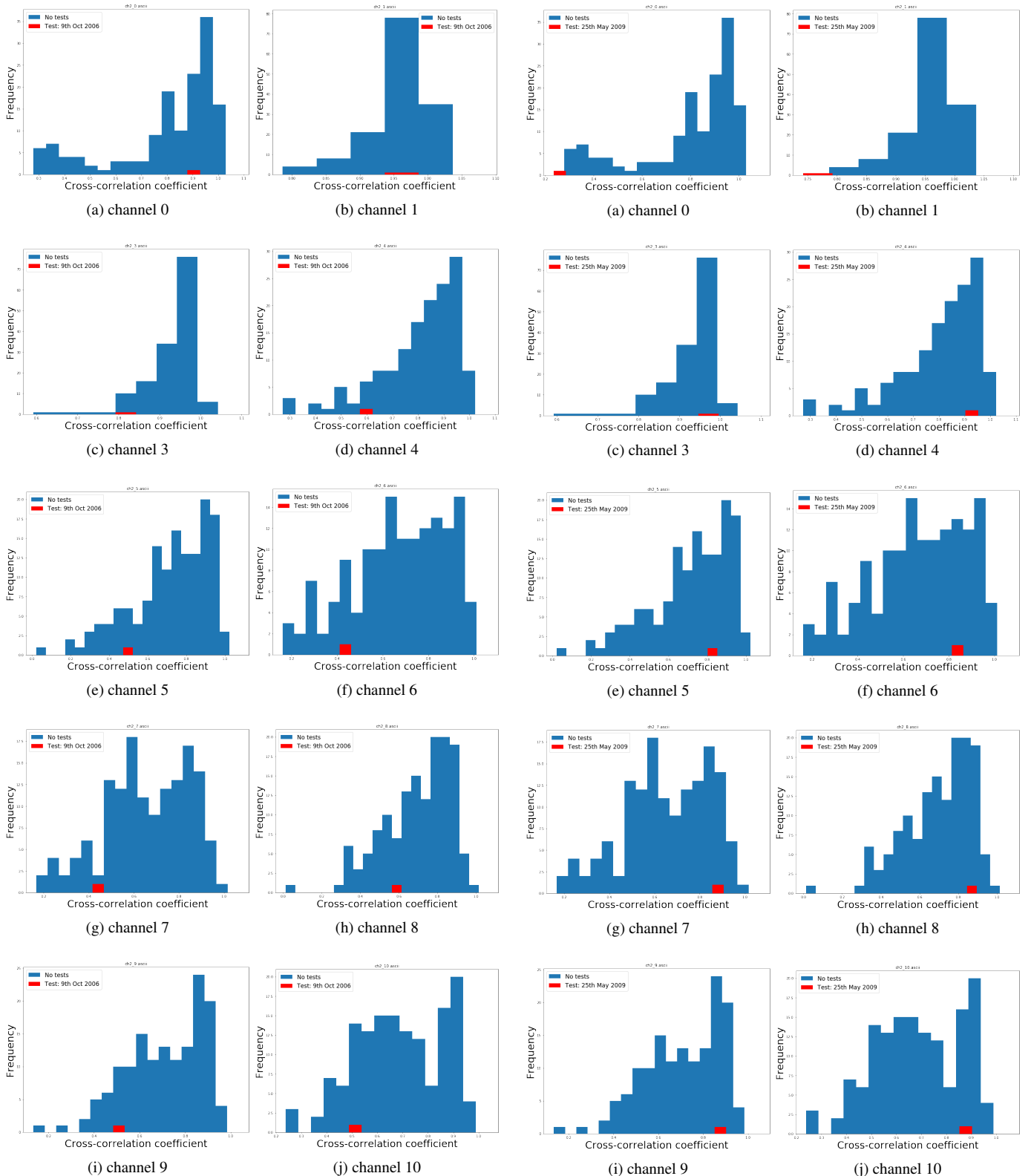


FIG. 12. Normalised cross–correlation coefficients of channel 2 for October 2006 test – satellite ns56.

FIG. 13. Normalised cross–correlation coefficients of channel 2 for May 2009 test – satellite ns56.

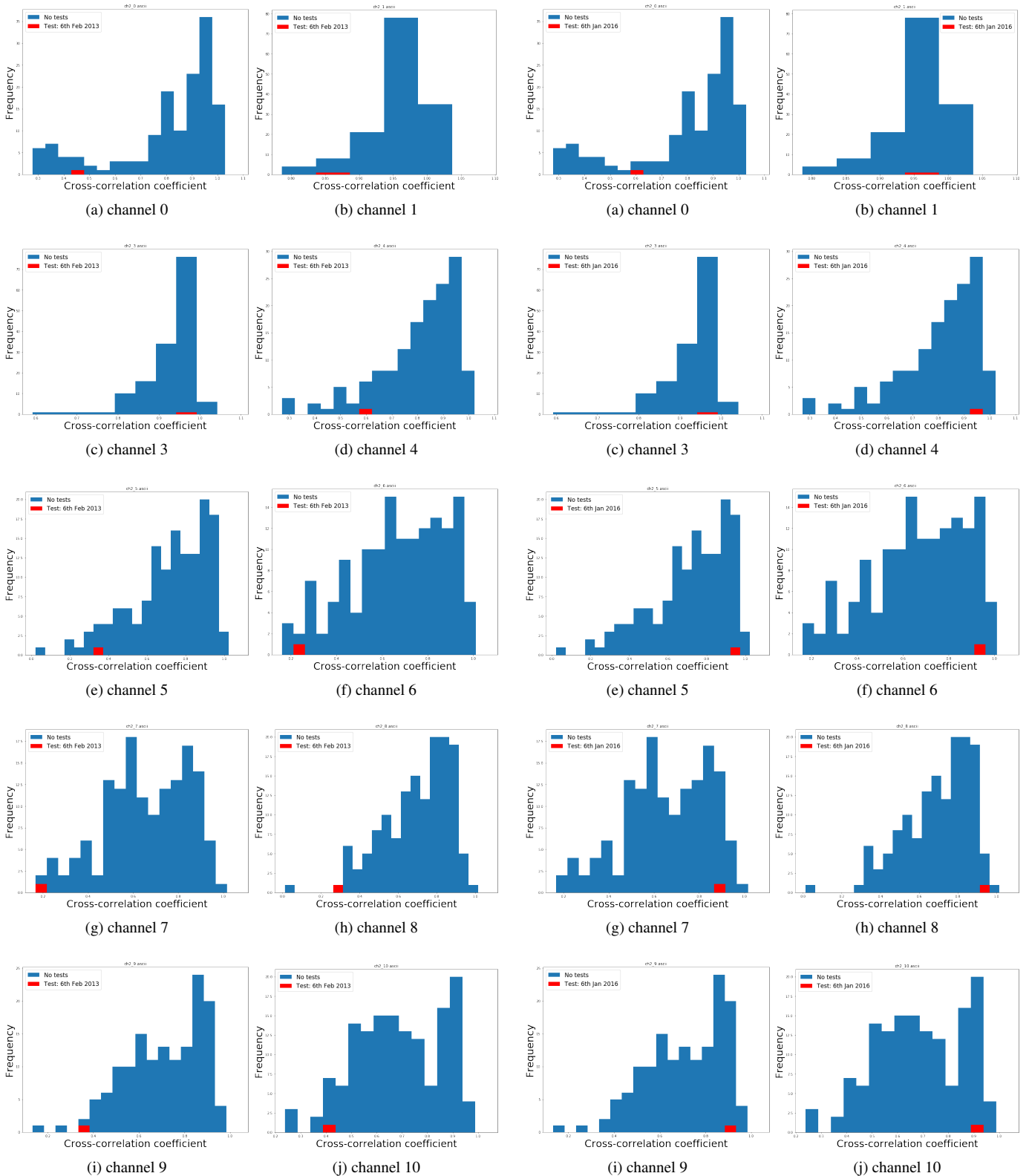
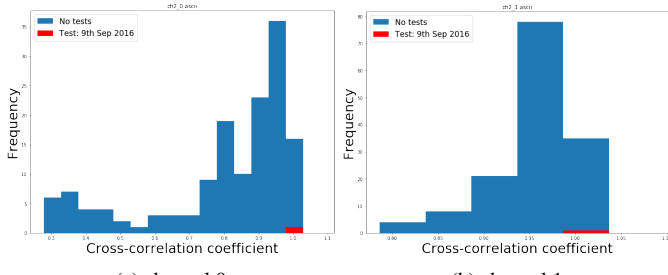
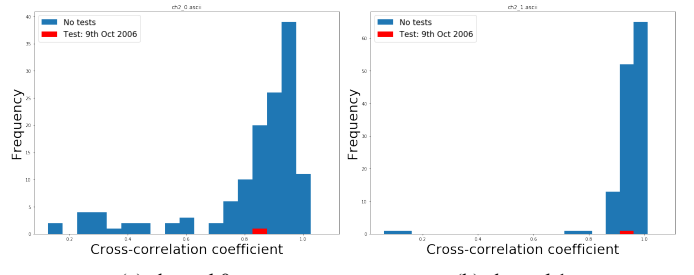


FIG. 14. Normalised cross–correlation coefficients of channel 2 for February 2013 test – satellite ns56.

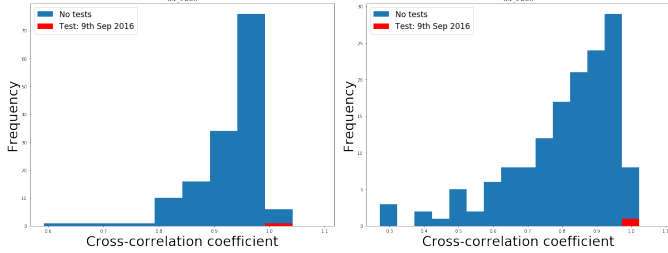
FIG. 15. Normalised cross–correlation coefficients of channel 2 for January 2016 test – satellite ns56.



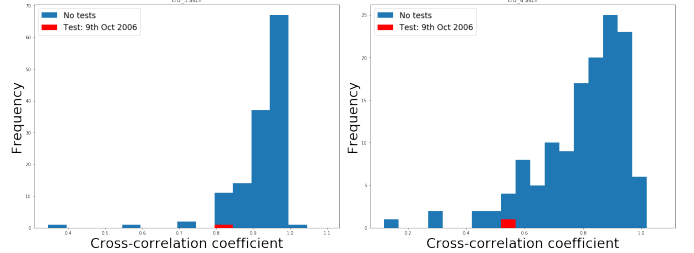
(a) channel 0



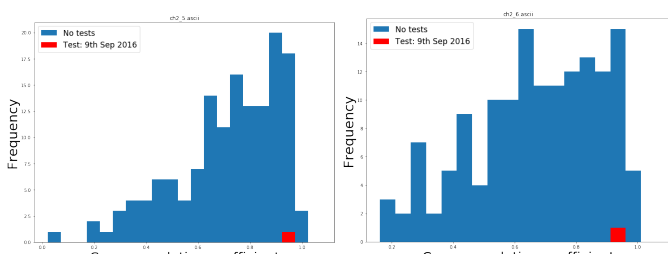
(a) channel 0



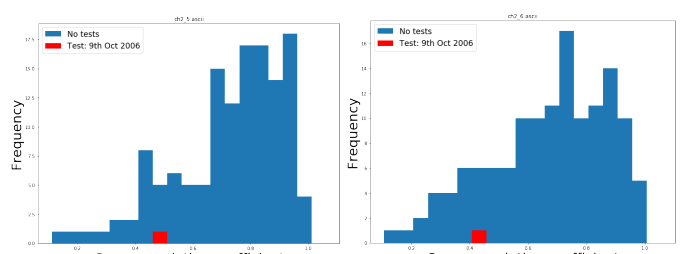
(c) channel 3



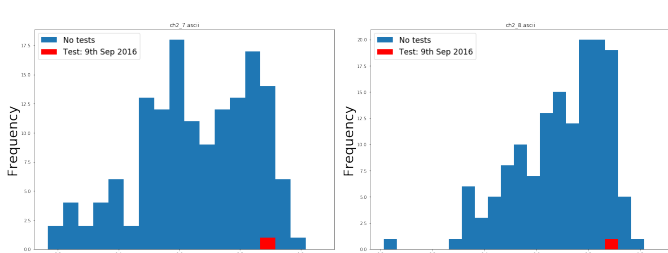
(c) channel 3



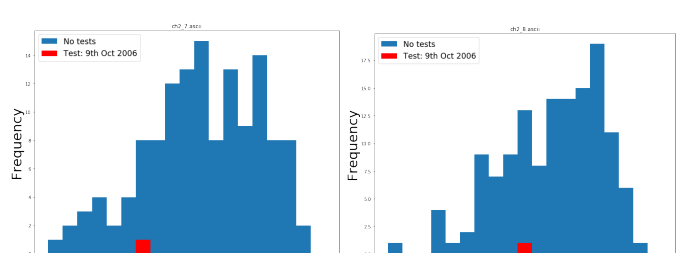
(a) channel 5



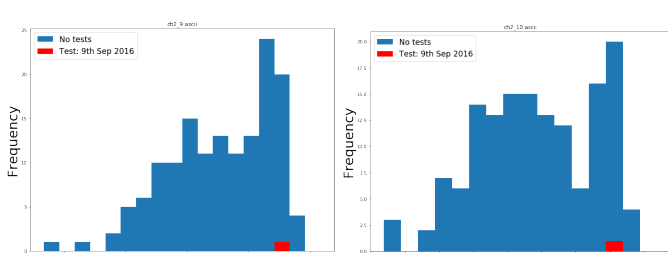
(a) channel 5



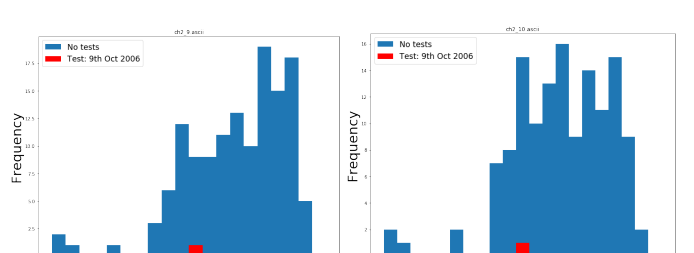
### Cross-correlation coefficient



### Cross-correlation coefficient



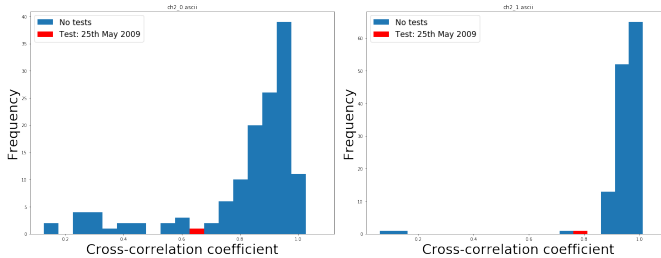
cross-correlation coe



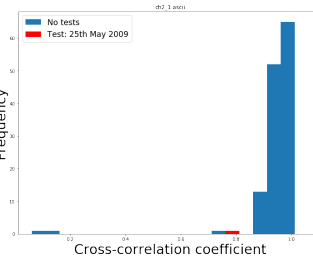
cross-correlation coe

FIG. 16. Normalised cross-correlation coefficients of channel 2 for September 2016 as a function of

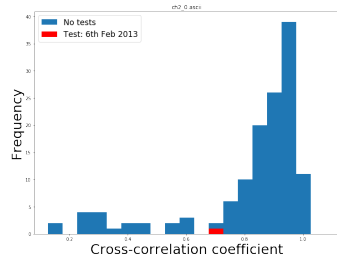
FIG. 17. Normalised cross-correlation coefficients of channel 2 for



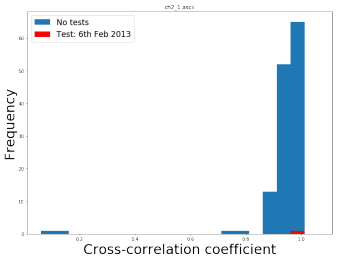
(a) channel 0



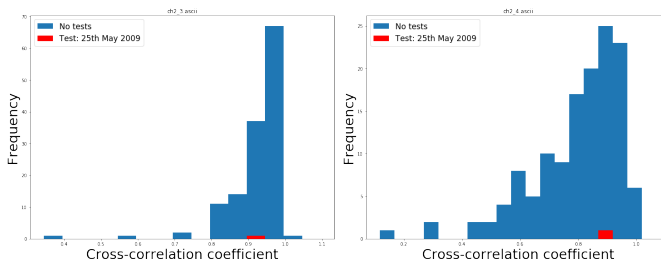
(b) channel 1



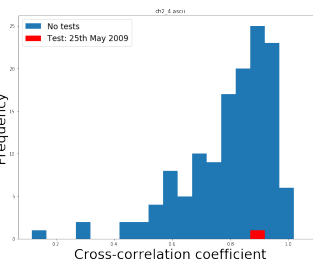
(a) channel 0



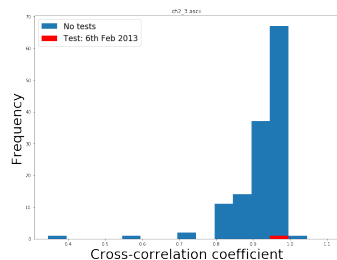
(b) channel 1



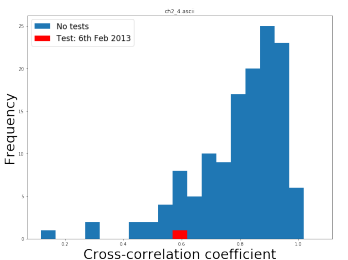
(c) channel 3



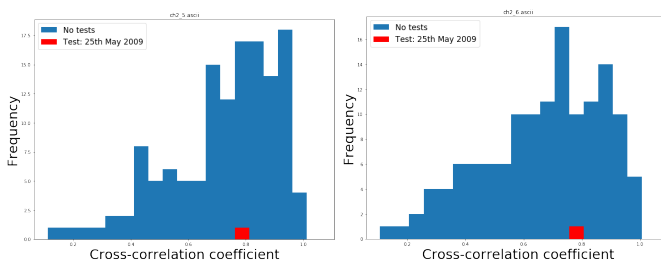
(d) channel 4



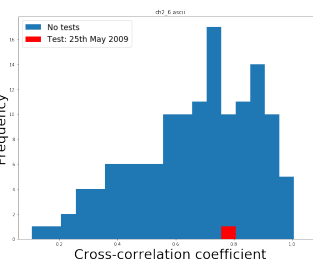
(c) channel 3



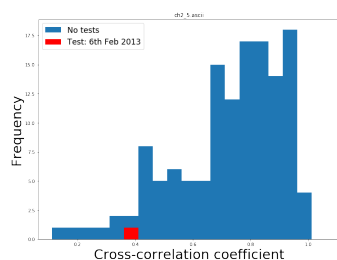
(d) channel 4



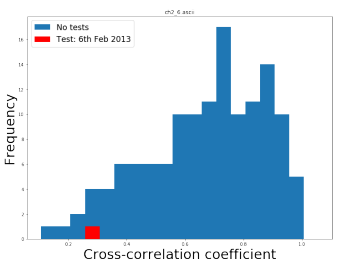
(e) channel 5



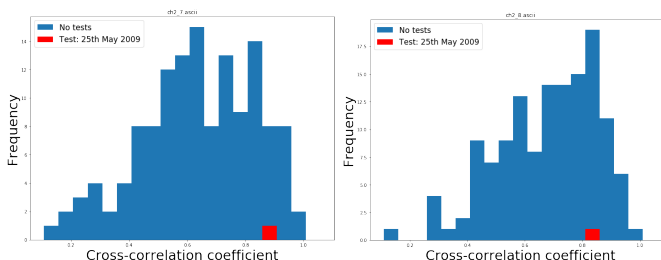
(f) channel 6



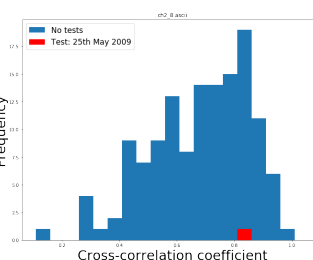
(e) channel 5



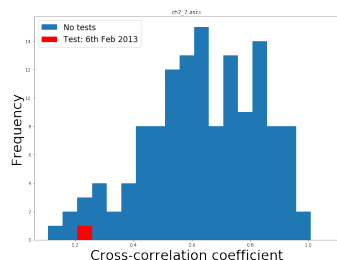
(f) channel 6



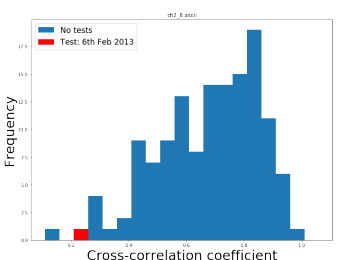
(g) channel 7



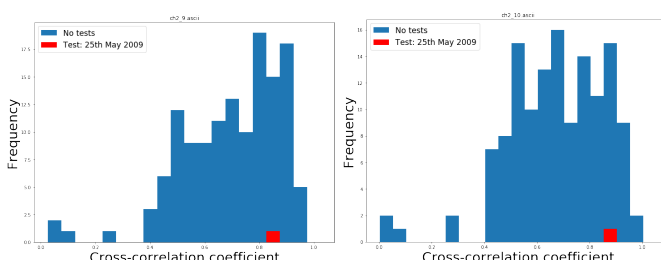
(h) channel 8



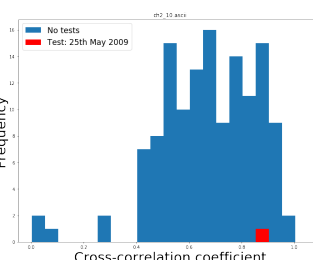
(g) channel 7



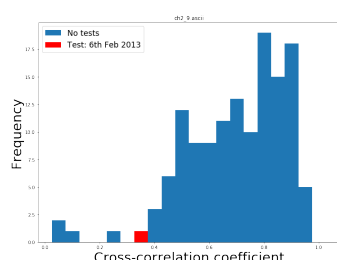
(h) channel 8



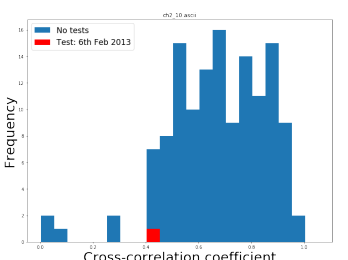
(i) channel 9



(j) channel 10



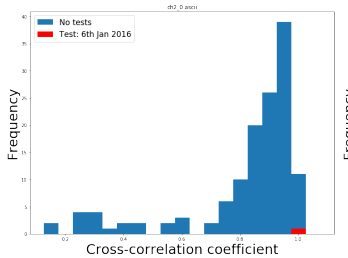
(i) channel 9



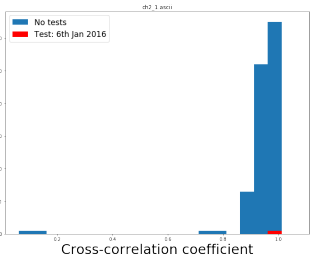
(j) channel 10

FIG. 18. Normalised cross-correlation coefficients of channel 2 for May 2009 test – satellite ns59.

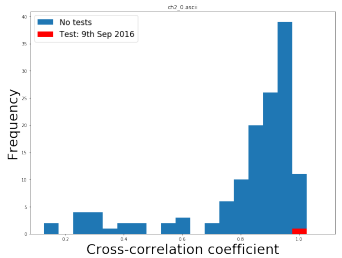
FIG. 19. Normalised cross-correlation coefficients of channel 2 for February 2013 test – satellite ns59.



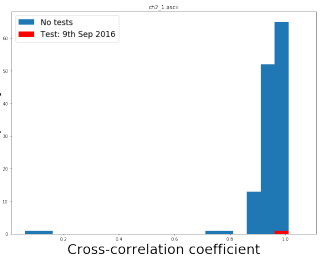
(a) channel 0



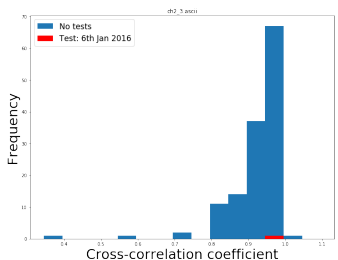
(b) channel 1



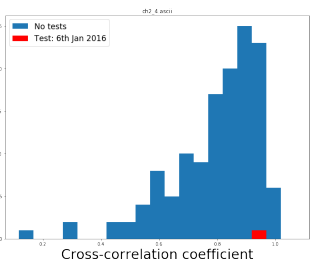
(a) channel 0



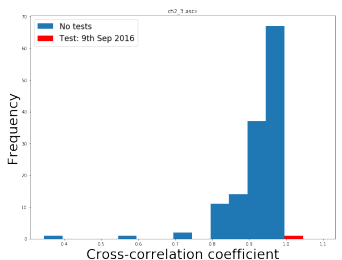
(b) channel 1



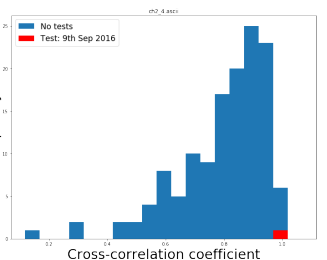
(c) channel 3



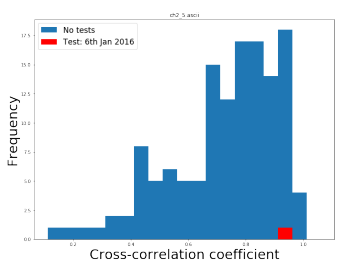
(d) channel 4



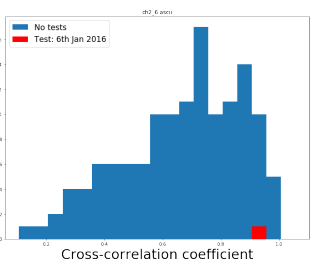
(c) channel 3



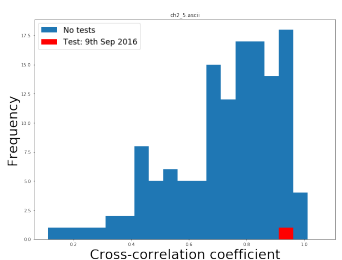
(d) channel 4



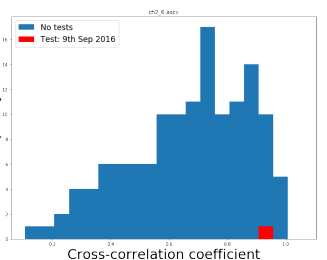
(e) channel 5



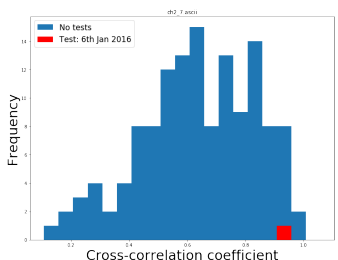
(f) channel 6



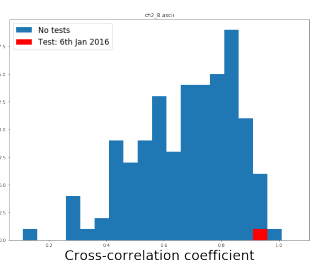
(e) channel 5



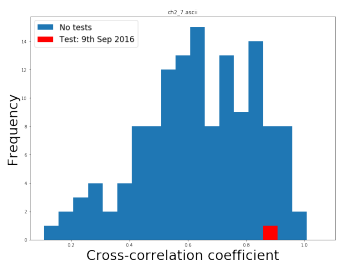
(f) channel 6



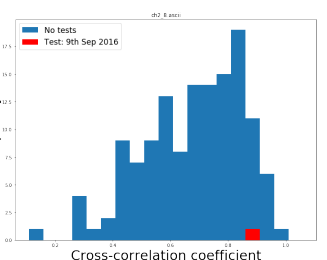
(g) channel 7



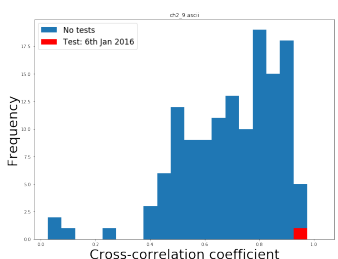
(h) channel 8



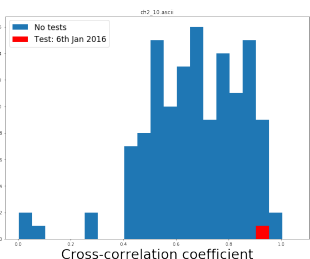
(g) channel 7



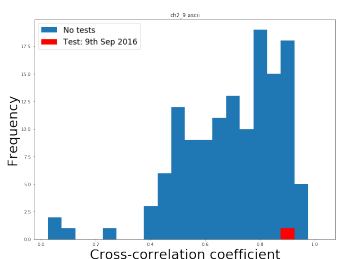
(h) channel 8



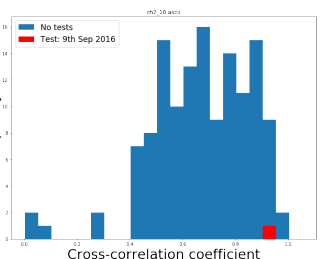
(i) channel 9



(j) channel 10



(i) channel 9



(j) channel 10

FIG. 20. Normalised cross-correlation coefficients of channel 2 for January 2016 test – satellite ns59.

FIG. 21. Normalised cross-correlation coefficients of channel 2 for September 2016 test – satellite ns59.



FIG. 22. Normalised cross-correlation coefficients of channel 2 for October 2006 test.

FIG. 23. Normalised cross-correlation coefficients of channel 2 for May 2009 test – satellite ns60.



FIG. 24. Normalised cross-correlation coefficients of channel 2 for February 2013 test – satellite ns60.

FIG. 25. Normalised cross-correlation coefficients of channel 2 for January 2016 test – satellite ns60.

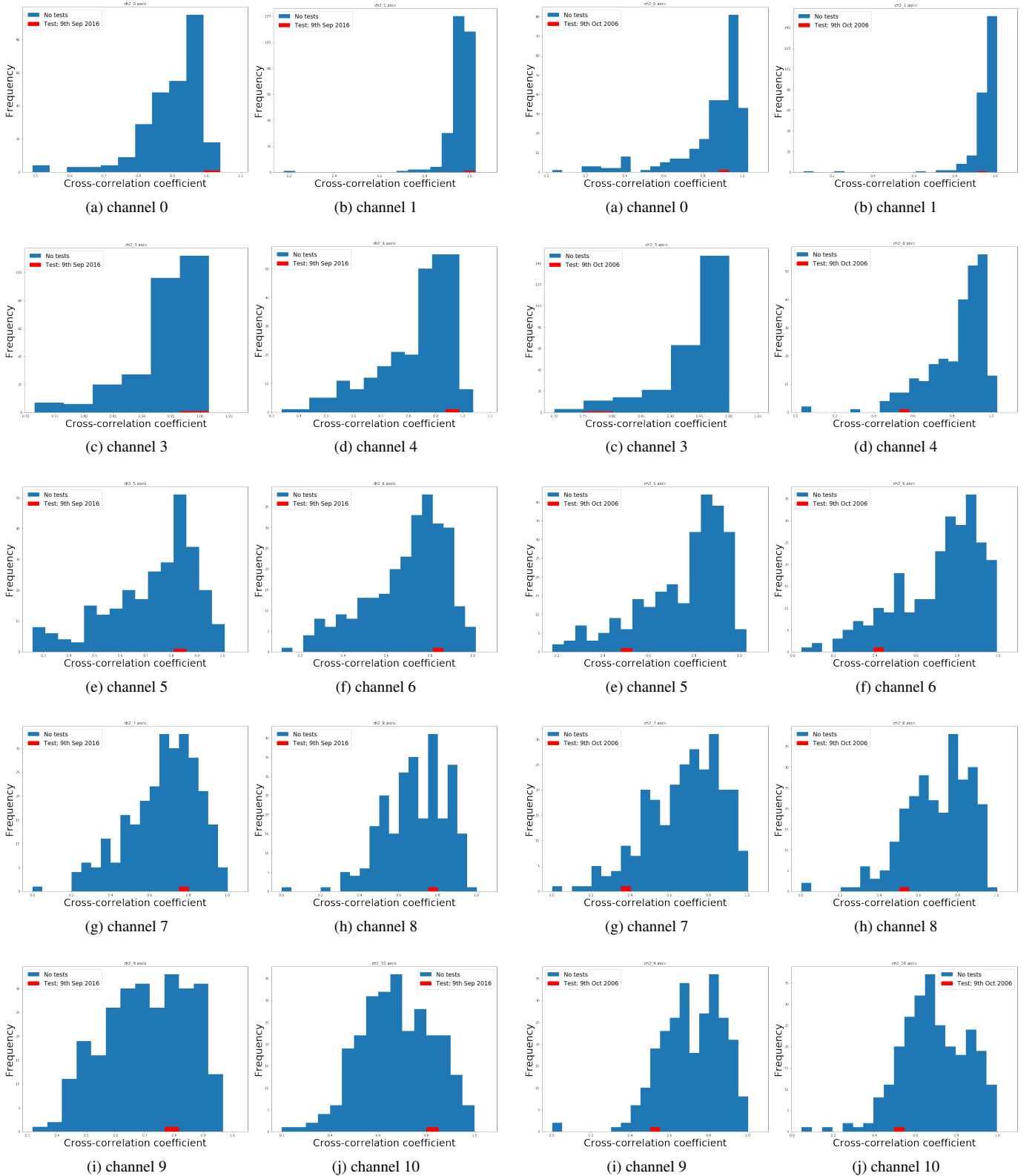


FIG. 26. Normalised cross-correlation coefficients of channel 2 for September 2016 test – satellite ns60.

FIG. 27. Normalised cross-correlation coefficients of channel 2 for October 2006 test – satellite ns61.

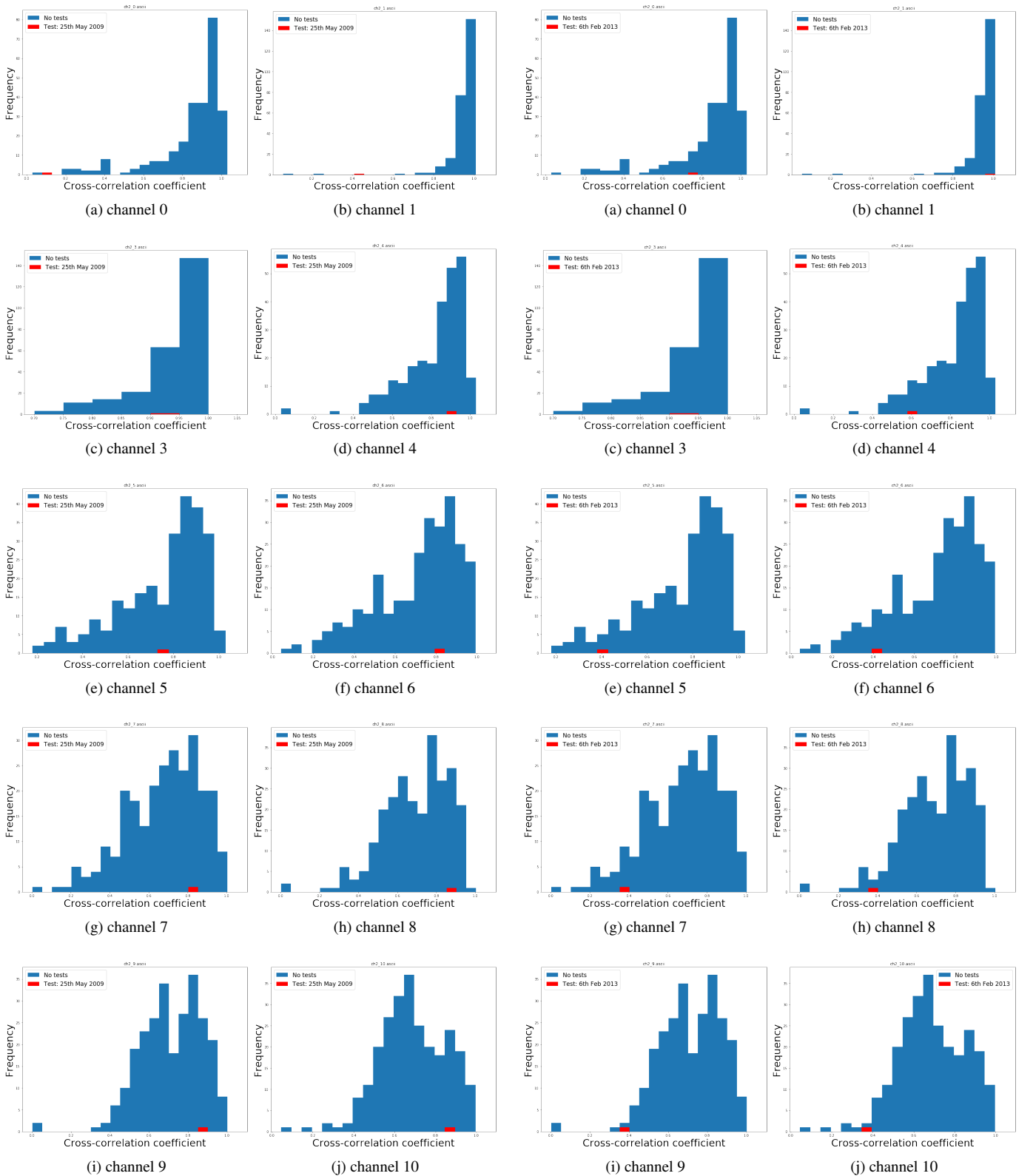


FIG. 28. Normalised cross-correlation coefficients of channel 2 for May 2009 test – satellite ns61.

FIG. 29. Normalised cross-correlation coefficients of channel 2 for February 2013 test – satellite ns61.

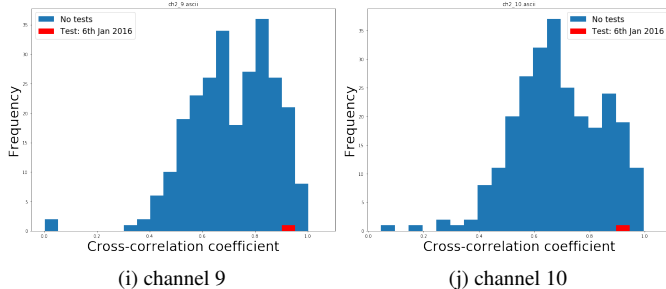
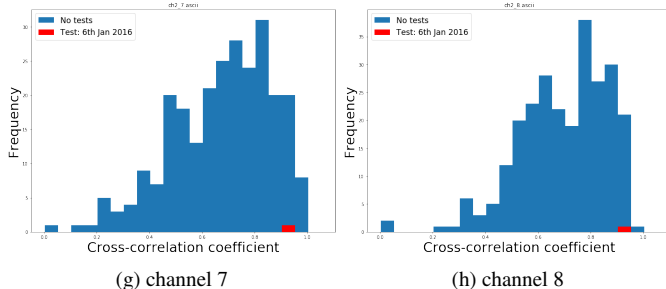
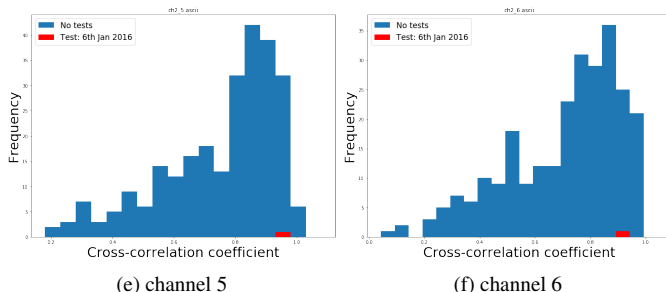
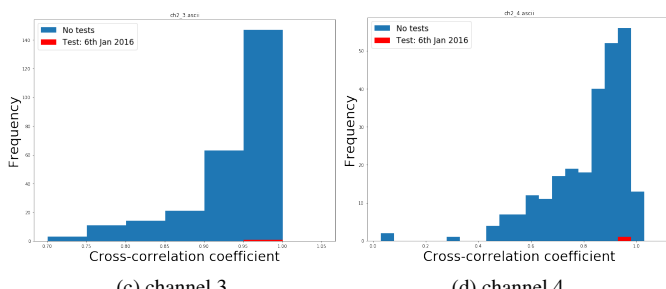
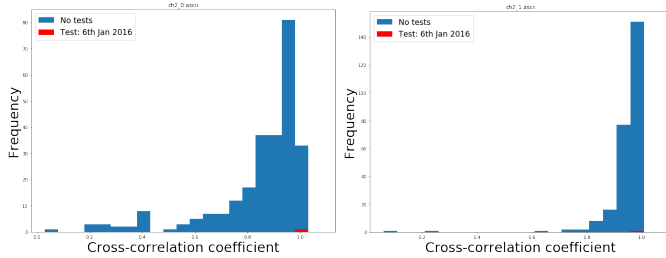


FIG. 30. Normalised cross-correlation coefficients of channel 2 for January 2016 test – satellite ns61.

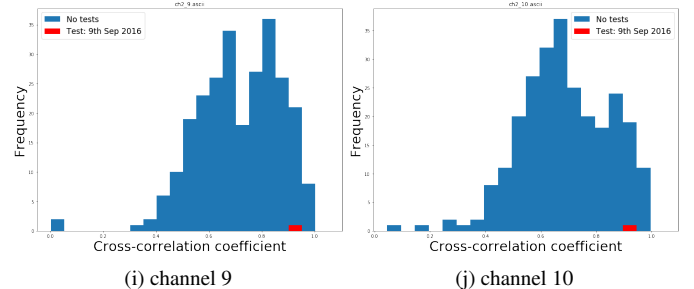
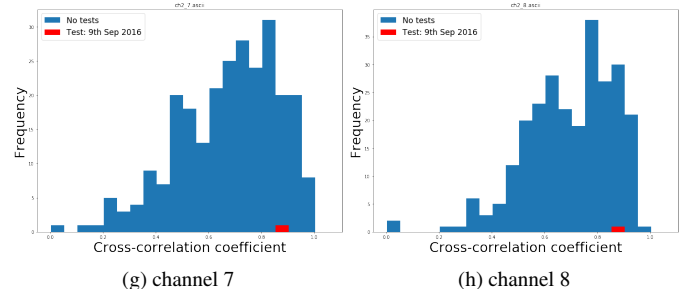
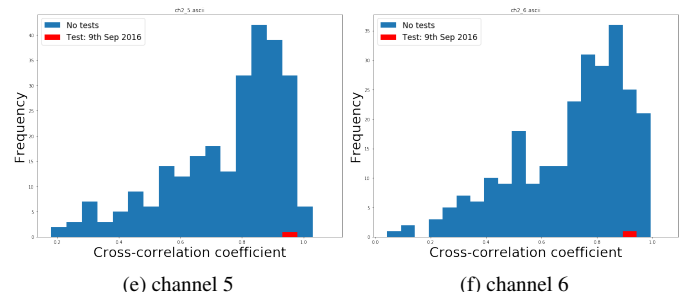
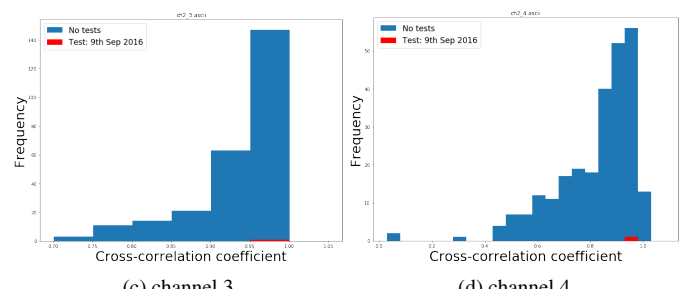
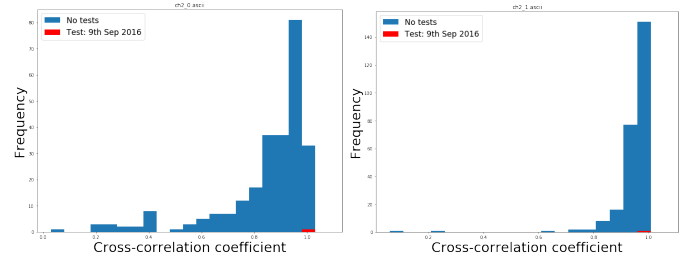


FIG. 31. Normalised cross-correlation coefficients of channel 2 for September 2016 test – satellite ns61.

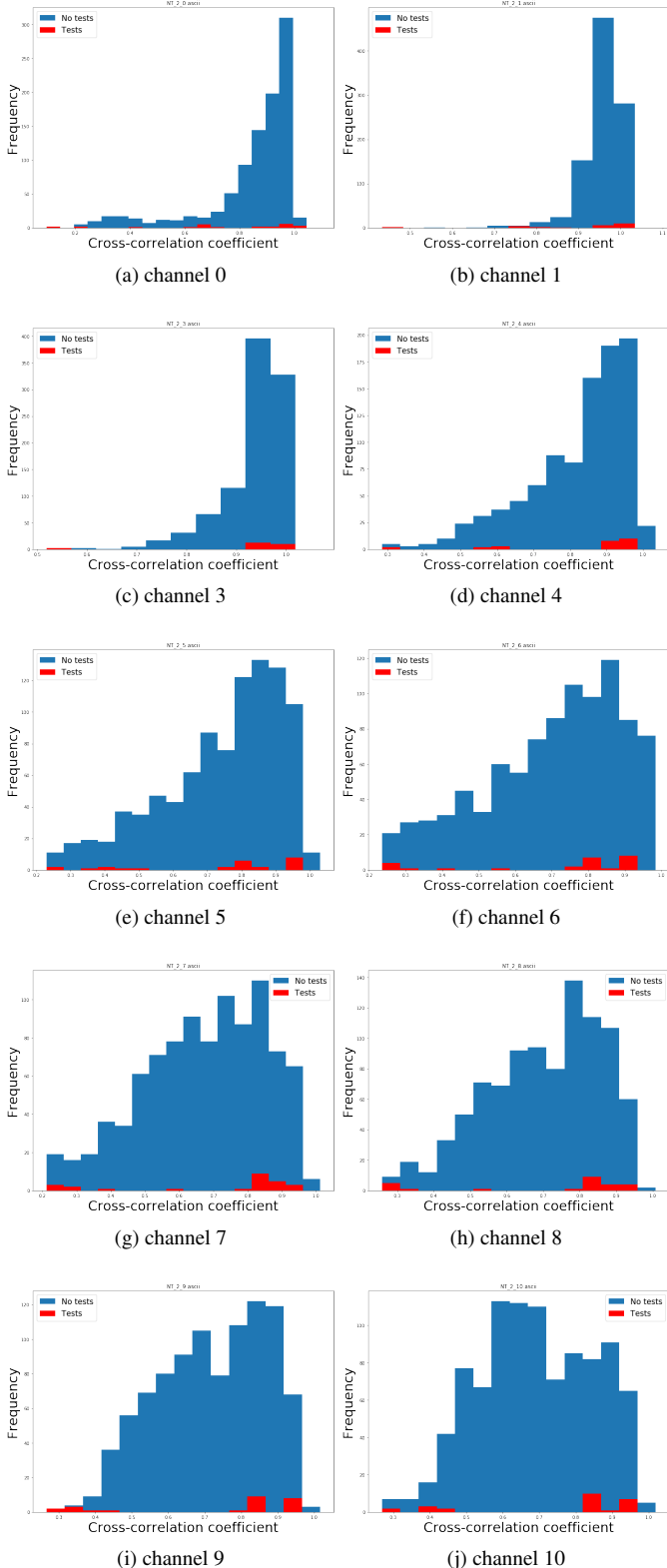


FIG. 32. Normalised cross-correlation coefficients resulting from merging distributions for satellites, ns: 54, 56, 59, 60 and 61.